General Methodology for Evaluating the Adhesion Force of Drops and Bubbles on Solid Surfaces

ARTICLE *in* LANGMUIR · JUNE 2009

Impact Factor: 4.46 · DOI: 10.1021/la804099z · Source: PubMed

5 AUTHORS, INCLUDING:

Carlo Antonini
Empa - Swiss Federal Laboratories for Materi…
42 PUBLICATIONS **367** CITATIONS
SEE PROFILE

Javier Carmona
Universidad de Extremadura
58 PUBLICATIONS **444** CITATIONS
SEE PROFILE

Marco Marengo
University of Brighton
156 PUBLICATIONS **1,364** CITATIONS
SEE PROFILE

Langmuir
Article
pubs.acs.org/Langmuir

General Methodology for Evaluating the Adhesion Force of Drops and Bubbles on Solid Surfaces

C. Antonini,[†,‡] F. J. Carmona,[†,§] E. Pierce,[†] M. Marengo,[‡] and A. Amirfazli*,[†]

[†]*Department of Mechanical Engineering, University of Alberta, Edmonton, AB, Canada T6G 2G8, and* [‡]*Dipartimento di Ingegneria Industriale, Università degli Studi di Bergamo, Viale Marconi 5, 24044 Dalmine (BG), Italy.* [§]*Current address: Dept. Fisica Aplicada, Universidad de Extremadura, 10071 Caceres, Spain*

Received December 12, 2008. Revised Manuscript Received March 23, 2009

The shortcomings of the current formulation for calculating the adhesion force for drops and bubbles with noncircular contact lines are discussed. A general formulation to evaluate the adhesion force due to surface forces is presented. Also, a novel methodology, that is, IBAFA, image based adhesion force analysis, was developed to allow implementation of the general formulation. IBAFA is based on the use of multiple profile images of a drop. The images are analyzed (1) to accurately reconstruct the contact line shape, which is analytically represented by a Fourier cosine series, and (2) to measure contact angles at multiple locations along the contact line and determine the contact angle distribution based on a linear piecewise interpolation routine. The contact line shape reconstruction procedure was validated with both actual experiments and simulated experiments. The procedure for the evaluation of the adhesion force was tested using simulated experiments with synthetic drops of known shapes. A comparison with current methods showed that simplifying assumptions (e.g., elliptical contact line or linear contact angle distribution) used in these methods result in errors up to 76% in the estimated adhesion force. However, the drop adhesion force evaluated using IBAFA results in small errors on the order of 1%.

1. Introduction

Understanding the incipient motion of a drop adhered to a surface has wide applications, from self-cleaning of superhydrophobic surfaces to electromagnetic drop actuation in microfluidic systems. When a drop is placed on an ideal horizontal surface, its shape is axisymmetric, so that the contact line (three-phase boundary) is circular and the contact angle distribution along the contact line is uniform. If an external force, such as gravity (on tilted surfaces) or aerodynamics (in shear airflows), is applied to such a resting drop, the contact line and/or contact angle distribution along the contact line must distort, if motion is to be resisted. This distortion is responsible for the adhesion force, which keeps the drop attached to the surface in the presence of the external force. As such, knowledge of the contact line shape and of the contact angle distribution along the contact line is fundamental to estimating the drop adhesion force. Figure 1a shows the profile of a drop on a tilted surface.

To determine whether the drop will move as a result of an external force, it is necessary to predict the drop adhesion force. The adhesion force is the manifestation of interfacial tension, γ, acting at the contact line.

Consider the case of a drop subject to an external force, such as gravity, whose component on the plane of the surface is oriented in the x-direction (see Figure 1a). In this case, the only component of the adhesion force, which is generally considered, is the one in the x-direction. As a result of this coordinate system convention, the external force component and, therefore, net adhesion force in the y-direction is null, whereas z-direction adhesion force is generally neglected, as drop movement in the z-direction is constrained by the surface. Consider Figure 1b, at each differential segment of the contact line, dl, the resisting force, dF_x, is given by

$$\mathrm{d}F_x = \gamma_x \,\mathrm{d}l \tag{1}$$

where γ_x is as defined in Figure 1b. Note that γ_x is a function of both the local contact line normal, ψ, and the contact angle, θ (see Figure 1b). By integrating eq 1 over the entire contact line, it is possible to calculate the force of adhesion in the x-direction from the surface tension, the contact angle distribution, and the contact line shape and length.

The procedure for adhesion force calculation can also be extended to bubbles attached to solid surfaces. The present paper focuses on drops, as they have been the subject of experimentation. However, it is important to underline that the following discussion and the proposed methodology apply equally to bubbles. Indeed, the physical mechanism that keeps a bubble attached to a solid surface is similarly due to surface tension forces as for drops.

Previous models to describe the drop adhesion acknowledge the basic principle that the drop shape deformation is important. However, they are generally limited by assumptions for contact line shape and contact angle distribution along the contact line.

With regards to the contact line, different ideal shapes have been used. The first proposed shape was a circular contact line, the same as for a drop sitting on an ideal smooth horizontal surface. Brown[1] assumed a circular contact line for the purposes of his finite element model, which predicted the contact angle distribution of a drop on an inclined surface. A circular contact line was

*Corresponding author. E-mail: a.amirfazli@ualberta.ca.

(1) Brown, R. A.; Orr, F. M.; Scriven, L. E. *J. Colloid Interface Sci.* **1980**, *73* 76–87.

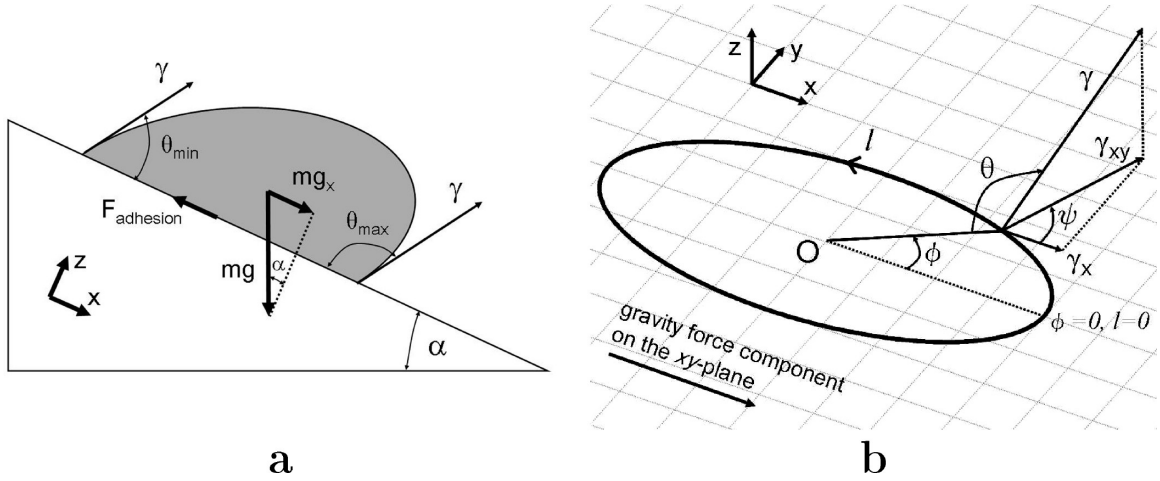

Figure 1. (a) Profile of a drop on a tilted surface. (b) View of the contact line; γ is the surface tension vector, γ_{xy} is its projection on the xy-plane, and γ_x is its component along the x-direction; θ is the contact angle, ψ is the angle normal to the contact line, ϕ is the azimuthal angle, and l is the curvilinear coordinate along the contact line; O is the origin of the coordinate system. Note that, for a noncircular shape, such as an ellipse, ψ and ϕ are generally not equivalent.

also assumed in the mathematical model of Quéré et al.,[2] which predicted the volume at which a very small spherical drop would move on an inclined surface. Dussan and Chow[3] developed a mathematical model, based on asymptotic theory, which was not limited to circular contact lines but was only valid for small contact angle hysteresis. This model was developed to predict the contact line shape and the speed at which the drop moves along the surface when the adhesion force is overcome by the external force. They modeled the contact line as two arc segments, named advancing and receding contact lines, connected by two straight-line segments. Bouteau et al.[4] used the same simplified contact line model to investigate the critical sliding angle of a drop placed on a surface. In ref 4, for the system studied, it was concluded that the "parallel-sided elongated drop" provided a better agreement with experimental observations than that of elliptical or circular contact line models, except for the highest values of the contact angle hysteresis. However, the results indicate that as it stands the current contact line models are too specific for a general system (e.g., the drops in Figure 2) and there is a need for developing a more general representation for the contact line. Extrand and Kumagai[5] approximated the contact line of a drop at incipient motion as an ellipse. Using a series of profile images, captured by a camera, which rotated around the drop, ElSherbini and Jacobi[6,7] observed that a double-ellipse model provided a good approximation for the contact line of a drop at incipient motion. However, they recommended that a single ellipse with an equivalent area leads to similarly good approximation of drop volume and adhesion force for the system studied. Therefore, a single ellipse was used in ref 6 to represent the contact line.

These simplified models of contact line shape may not always be adequate, especially in experiments involving surfaces with anisotropic topography,[8] which is the case for many industrial grade materials. Drops placed on such surfaces often exhibit

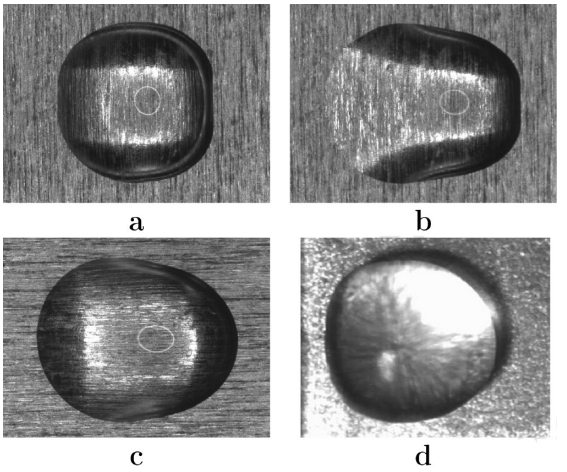

Figure 2. Four different examples of the contact line shapes. Images were recorded from the top of the drop. The view of the contact line was possible as the contact angle is lower than 90°. (a, b) A 15 μL drop of bromonaphthalene on mill finished aluminum at different inclination of the surface; the external force is gravity. (c) Same as (a) and (b), with a different orientation for the surface. (d) A 40 μL water drop on PMMA, exposed to an air shear flow. The direction of the external force is from left to right in all cases.

contact line shapes that are not well represented by a circular or elliptical approximation, as illustrated in Figure 2.

With regards to mathematical representations of the contact angle distribution along the contact line, different models have been proposed in the literature. All the models are based either on the knowledge of the advancing and receding contact angles, or on the maximum and minimum contact angles. The advancing and receding contact angles, θ_A and θ_R, are the contact angles measured on a horizontal surface while expanding and contracting a drop, respectively. The maximum and minimum contact angles, θ_{max} and θ_{min}, are the contact angles measured on a surface inclined to the sliding angle at the leading and trailing edge, respectively. In refs 5 and 9, θ_{max} and θ_{min} are assumed to be equal to θ_A and θ_R, respectively. There are however theoretical[10] and experimental[11] arguments that indicate the advancing angle

(2) Quéré, D.; Azzopardi, M. J.; Delattre, L. *Langmuir* **1998**, *14*, 2213–2216.
(3) Dussan, E. B.; Tao-Ping Chow, R. *J. Fluid Mech.* **1983**, *137*, 1–29.
(4) Bouteau, M.; Cantin, S.; Benhabib, F.; Perrot, F. *J. Colloid Interface Sci.* **2008**, *317*(1), 247–254.
(5) Extrand, C. W.; Kumagai, Y. *J. Colloid Interface Sci.* **1995**, *170*(2), 515–521.
(6) ElSherbini, A. I.; Jacobi, A. M. *J. Colloid Interface Sci.* **2004**, *273*(2), 556–565.
(7) ElSherbini, A. I.; Jacobi, A. M. *J. Colloid Interface Sci.* **2004**, *273*(2), 566–575.
(8) Sommers, A. D.; Jacobi, A. M. *J. Micromech. Microeng.* **2006**, *16*(8), 1571–1578.
(9) Blackmore, B.; Li, D.; Gao, J. *J. Colloid Interface Sci.* **2001**, *241*(2), 514–520.
(10) Krasovitski, B.; Marmur, A. *Langmuir* **2005**, *21*(9), 3881–3885.
(11) Pierce, E.; Carmona, F. J.; Amirfazli, A. *Colloids Surf., A* **2008**, *323*, 73–82.

may not necessarily be equal to the maximum contact angle; these studies similarly indicate that the receding contact angle will not be necessarily equivalent to the minimum angle observed even for the same surface−liquid combination.

The simplest proposed model[9] involved dividing the contact line into two sections. Each section is assumed to have a uniform contact angle, with one section having the advancing contact angle, θ_A, and one having the receding angle, θ_R. The angles θ_A and θ_R are measured on a level surface while expanding and contracting a drop, respectively. Extrand and Kumagai[5] assumed that the distribution of the contact angle cosine, cos θ, varies linearly with respect to the azimuthal angle, ϕ (see Figure 1b), ranging from θ_A to θ_R.

Examining multiple profile images of a drop from different azimuthal orientations, ElSherbini and Jacobi[6,7] measured the contact angle distribution along the contact line of drops on tilted surfaces. For the systems studied, they concluded that the overall contact angle distribution along the contact line could be described as a function of the contact angles at the trailing and the leading edge of the drop profile, θ_{min} and θ_{max}, on a surface inclined to the sliding angle (see Figure 1a). Note that θ_{min} and θ_{max} are simultaneously observed when the line of sight for the camera is parallel to the y-direction. In ref 6, the contact angle distribution, $\theta(\phi)$, or its cosine, cos $\theta(\phi)$, along the azimuthal angle, ϕ, was found to be adequately expressed as a third-degree polynomial function of θ_{min} and θ_{max}.

In ref 12, it is shown that a third order polynomial interpolation is inadequate on microgrooved surfaces, because the contact angle distribution is not monotonic; the maximum contact angle is found at an azimuthal angle $\phi = 90°$ and not at the leading edge. Therefore, it was necessary to define a case specific and complex contact angle distribution.

If the contact line shape and the contact angle distribution along the contact line are provided, it is possible to calculate the drop adhesion force. The force is computed by integration of the differential force dF_x, defined in Equation 1. However, a simplified expression can be found in literature. As an example, in [5] the following expression was used:

$$\frac{F_{adh,max}}{\gamma R} = k(\cos\theta_R - \cos\theta_A) \quad (2)$$

where R is a length scale for the contour of the drop and k is an adjustable parameter based on experimental data. This simplified formulation requires only the knowledge of the receding and advancing contact angle, θ_R and θ_A, respectively. Two remarks can be made for this formulation. First, in light of the findings of refs 10 and 11, eq 2 should be redefined as eq 3:

$$\frac{F_{adh,max}}{\gamma R} = k(\cos\theta_{min} - \cos\theta_{max}) \quad (3)$$

because the minimum and maximum contact angles, θ_{min} and θ_{max}, respectively, do not necessarily coincide with the receding and advancing contact angles, θ_R and θ_A, defined for a drop on a horizontal surface. Second, the introduction of the adjustable parameter k is necessary to fit the formulation to experimental data. It should be expected that the adhesion force cannot be adequately represented only by θ_{min} and θ_{max}, since it depends both on the contact line (shape and length) and on the contact angle distribution along the contact line. The advantage of using such a simplified formulation is that the adhesion force can be predicted accurately for a given liquid−surface combination once k is known for that system. The disadvantage is that an experimental calibration of k is required whenever either the surface or the liquid is changed.

According to a recent study,[13] the time a drop rests on a surface may cause a variation of the contact angle distribution and therefore influences the adhesion force. From experiments, the adhesion force is observed to increase with resting time on the order of minutes.[13] The automated apparatus used to capture multiple profile images is capable of recording images in a few seconds. Thus, it can be assumed that drop shape variation as well as evaporation[11] are negligible for the time needed for image acquisition.

This study proposes a new methodology, image based adhesion force analysis (IBAFA), to accurately evaluate the drop adhesion force by recording multiple profile images of a drop. Results show that the proposed methodology allows an accurate reconstruction of both the contact line shape and the contact angle distribution along the contact line. In particular, the application of the IBAFA does not require any assumption for either the contact line shape (e.g., circular or elliptical) or the advancing/maximum and receding/minimum values that are seen at the moment of incipient motion. In fact, IBAFA can be used to study any drop attached to a surface and not only to study drops at the condition of incipient motion, when the contact angles values reach the minimum/maximum or advancing/receding limits. As a direct consequence, the adhesion force can be evaluated with a high level of accuracy. The adhesion of bubbles to surfaces can also be investigated in a similar way. Furthermore, IBAFA can be a valuable tool in studies similar to that in ref 10, where time effect has to be investigated. By recording drop multiple profile images at different time steps, variation of the contact line, of the contact angle distribution along the contact line, and of the adhesion force can be measured and evaluated.

Although the proposed methodology will be discussed in terms of tilted surface experiments, it can be applied to any number of other cases, for example, the incipient motion of a drop in shear fluid flows. Understanding this phenomenon is significant to applications such as fuel cells,[14] aircraft icing,[15] and enhanced oil recovery.[16] With regards to bubbles, the bubble adhesion to the solid surface is of interest in studies of heat transfer in multiphase flows and shear-driven flows.

2. Adhesion Force

Consider a drop subjected to an external force, such as gravity, in a static condition (see Figure 1a). The only force acting on the drop in the x-direction, aside from the external force, is the adhesion force due to interfacial forces. The shear force between the fluid and the solid will be zero, since there is no motion.

It was found that the original formulation for the drop adhesion force, presented in ref 1, has been misinterpreted in the literature. The adhesion force is given by the integral of the component of the surface tension force, projected in the external force direction (see Figure 1b and eq 1). In ref 1, the adhesion force was given only for a drop with a circular contact line as

$$F_{adhesion} = F_x = -\gamma \int_0^{2\pi} r\cos\theta(\phi)\cos\phi\, d\phi \quad (4)$$

(12) Sommers, A. D.; Jacobi, A. M. *J. Colloid Interface Sci.* **2008**, *328*, 402–411.

(13) Yadav, P. S.; Bahadur, P.; Tadmor, R.; Chaurasia, K.; Leh, A. *Langmuir* **2008**, *24*(7), 3181–3184.

(14) Kumbur, E. C.; Sharp, K. V.; Mench, M. M. *J. Power Sources* **2006**, *161*(1), 333–345.

(15) Lee, S.; Bragg, M. B. *J. Aircr.* **1999**, *36*, 844–850.

(16) Mahé, M.; Vignes-Adler, M.; Rousseau, A.; Jacquin, C. G.; Adler, P. M. *J. Colloid Interface Sci.* **1988**, *126*, 314–328.

where γ, ϕ, and $\theta(\phi)$ have been previously defined and $r = r(\phi)$ describes the contact line. Although eq 4 is only valid for drops with circular contact lines, this expression was later presented in refs 5 and 17, where it was applied to models with elliptical contact line shapes. Recalling that interfacial tension forces are normal to the contact line, eq 4 assumes that the normal to the contact line (ψ in Figure 1b) is equal to the azimuthal angle, ϕ, which is only true for circular contact lines. Furthermore, eq 4 implies that the differential segment of the contact line dl (see eq 1) is equal to $r\,d\phi$, which again is only applicable to circles. For a generic curve, the correct expression for the differential segment length is $dl = (r^2 + r'^2)^{1/2}\,d\phi$, where r' is the first derivative of r with respect to ϕ.

In ref 12, Sommers and Jacobi proposed a new formulation for the case of a parallel sided elongated drop. In their new formulation, it is acknowledged that the normal to the contact line, ψ, differs from the azimuthal angle, ϕ. However, in this new formulation, the differential length is still calculated as $r\,d\phi$. Thus, the adhesion force is not evaluated properly. Again, taken collectively, the recent results (e.g., refs 4 and 12) point to a need for a general treatment of the contact line shape to avoid the necessity of defining various case specific contact line models.

For these reasons, the general analytical expression for the adhesion force must be defined as

$$F_{\text{adhesion}} = F_x = \int_0^L \gamma_x\,dl = -\gamma \int_0^L \cos\theta(l)\cos\psi(l)\,dl \tag{5}$$

where L is the total length of the contact line, $\psi(l)$ is a function describing the distribution of the normal to the contact line, and $\theta(l)$ is a function describing the contact angle distribution along the contact line, with each being expressed in terms of the curvilinear coordinate l (see Figure 1b). The l is measured from the leading edge of the contact line (where $l = 0$) in the counterclockwise direction (see Figure 1b). The azimuthal angle, ϕ, is often used in the literature as the independent variable. To be consistent, eq 5 was reformulated as eq 6 below:

$$F_{\text{adhesion}} = -\gamma \int_0^{2\pi} \cos\theta(\phi)\cos\psi(\phi)\sqrt{r^2 + r'^2}\,d\phi \tag{6}$$

Equation 6 simplifies to eq 4 for circular shapes, since for this case $\psi = \phi$ and $dl = r\,d\phi$.

Thus, to compute the adhesion force, it is necessary to know (1) the contact line shape, from which $\psi(\phi)$ is derived, and (2) the contact angle distribution along the contact line, $\theta(\phi)$.

3. Perspective Error

The methodology proposed in this paper to determine adhesion force of a drop depends on having multiple profile images from different azimuthal positions. As already highlighted in ref 6, when drop profile images are used, there is a perspective error associated with the identification of the contact point coordinates. The perspective error can be understood with the help of Figure 3b. In a profile image taken at azimuthal angle ϕ, the camera will not record the "original coordinates" of the contact points (r_ϕ, ϕ) but (r_ω, ω), which are labeled as "recorded coordinates" (see Figure 3b). The recorded radius, r_ω, is the projection of the original radius, r_ϕ, on the viewing plane of the camera. This perspective error will not be present if the contact line is a circle, as in this particular case $\omega = \phi$, or if the line of sight for the camera is parallel to either the x- or y-direction. To correct the perspective error and find the correct contact point coordinates (r_ϕ, ϕ) from a set of recorded coordinates (r_ω, ω), a mathematical representation of the contact line must be specified. This representation is discussed in section 5.1. Simulated experiments were especially useful in quantitatively evaluating the effect of perspective error on the proposed drop shape reconstruction method.

4. Methods and Materials

In this study, both experimental and numerical tests were performed. During the experimental tests, images of a drop placed on a tilted surface were recorded by a camera, which rotated 180° around the drop, capturing profile images at 10° intervals and thus obtaining 18 images. The equipment consisted of custom-built hardware equipped with a rotating camera (A302f, Basler AG) and a 10 W halogen light source along with a diffuser for back lighting. To capture top views of the drop, another digital camera (XD700, Sony) was mounted above the drop, so that it tilted with the surface, maintaining a line of sight perpendicular to the surface at all times. Inclination of the stage was measured using a two-axis inclinometer (TSD-90, Instruments & Control Inc.). Both surface inclination and camera rotation were motorized and synchronized with image capture through computer control. To obtain an unobstructed image of the contact line in the top view camera, different surface/liquid combinations were chosen so that the contact angle was never greater than 90°. The surface selections were mill finished aluminum and PMMA, and liquids bromonaphthalene and water were used. Before use, surfaces were all cleaned using 95% acetone in a sonicator, dried, and rinsed with distilled water. The surfaces were dried before experiments. Drops were placed on horizontal surfaces that were then subsequently tilted. However, the apparatus also allows one to place drops on already tilted surfaces.

Simulated experiments with synthetic drops were implemented numerically to further test the capability of the proposed methodology, IBAFA. These simulations avoid the experimental uncertainties and allow the comparison with drop shape models that have known analytical solutions, as the contact line shape and the contact angle distribution can be derived analytically. In addition, synthetic drops with a contact angle greater than 90° provide a more challenging study case, as they may represent drops on superhydrophobic surfaces. The simulated experiment approach has been used in various studies, for example, refs 18−20.

As test cases, two different synthetic drops were used: (1) axes-inclined ellipsoids, labeled as x-symmetric drops (see Figure 4) and (2) axes-aligned ellipsoids, labeled as xy-symmetric drops (see Figure 5). An ellipsoid surface may not necessarily satisfy the Young−Laplace equation, which governs the shape of any liquid−vapor interface. However, this fact does not affect the aim of the present study, that is to evaluate a methodology based on the use of a series of profile images. The critical point is to understand whether the proposed methodology is able to accurately reconstruct the geometry of a 3D shape. Ellipsoids were chosen, because they provide elliptical contact lines, which have been used in the latest studies to fit the experimental drop contact lines;[5−7] thus, methodologies in the literature can be applied to such shapes and their results can be evaluated.

The x-symmetric synthetic drop is representative of drops subject to an external force in the x-direction, for example, on a tilted surface or in a shear airflow, as they may provide a nonzero adhesion force only in the x direction. An xy-symmetric synthetic drop cannot be practically achieved on a tilted surface, since the total net adhesion force is zero in both x- and y-directions, due to symmetry with respect to x- and y-axes. However, it may be of practical interest for drops subject to an external anisotropic force

(17) ElSherbini, A. I.; Jacobi, A. M. *J. Colloid Interface Sci.* **2006**, *299*(2), 841–849.
(18) Jennings, J. W.; Pallas, N. R. *Langmuir* **1988**, *4*(4), 959–967.
(19) Song, B.; Springer, J. *J. Colloid Interface Sci.* **1996**, *184*, 64–76.
(20) Amirfazli, A.; Graham-Eagle, J.; Pennell, S.; Neumann, A. W. *Colloids Surf., A* **2000**, *161*, 63–74.

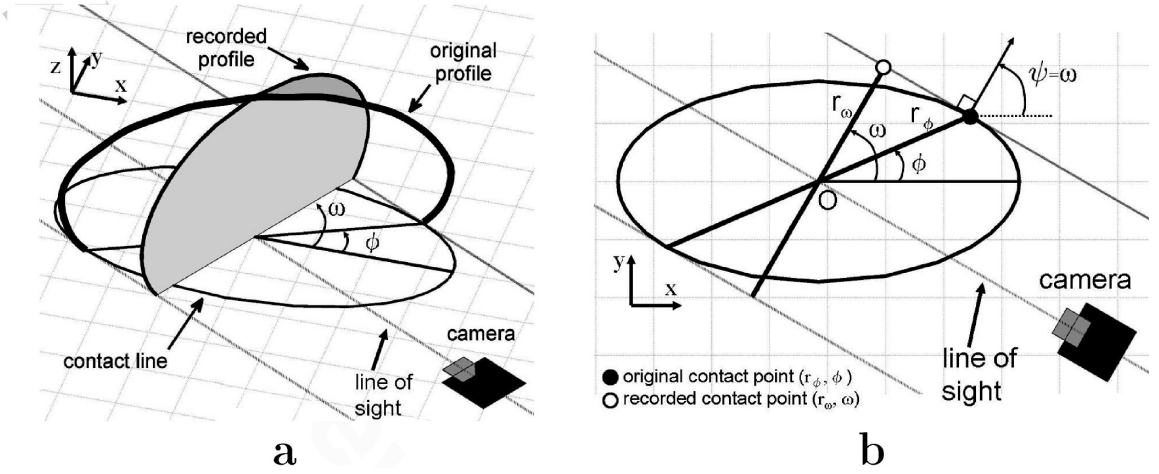

Figure 3. (a) Profile recorded by the camera (shaded), shown together with the original profile (thick line). The original profile is from the synthetic drop shown in Figure 5. (b) Top view of the ideal elliptical contact line. Due to perspective error, the contact point coordinates for the recorded profile will be (r_ω, ω) instead of (r_ϕ, ϕ) for the original profile. The coordinate origin is O. Note that, from basic trigonometry, the normal to the contact line, ψ, equals the recorded contact point angular coordinate, ω, for any general contact line; $\phi = \omega$ only for circular contact lines.

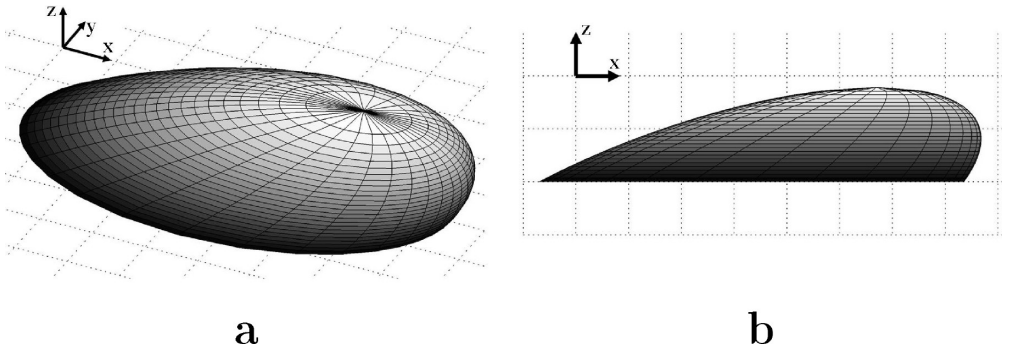

Figure 4. x-Symmetric drop, represented by a truncated inclined ellipsoid (semiaxes: $a = 3, b = 1.3, c = 1$, rotated by 20° around the y-axis). (a) 3D view and (b) profile, as seen on the xz-plane, showing maximum and minimum contact angles.

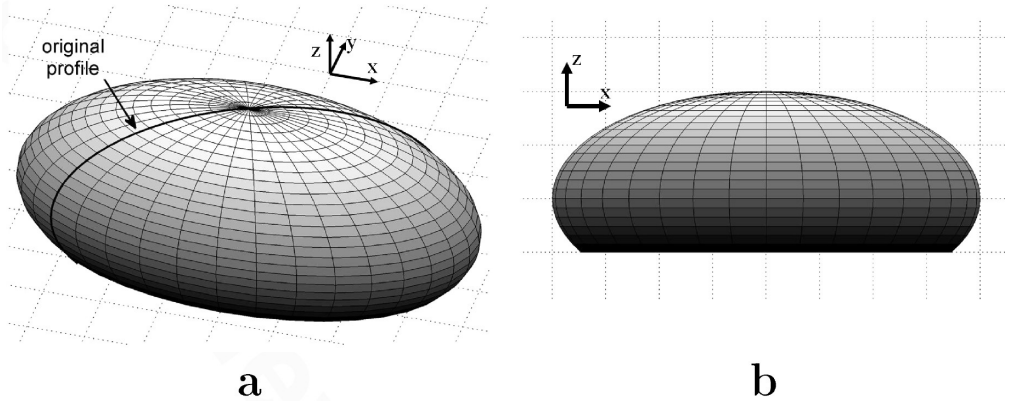

Figure 5. xy-Symmetric drop, represented by an ellipsoid truncated in the lower part to simulate drops with high contact angles (semiaxes: $a = 4, b = 2, c = 2$). (a) 3D view and (b) profile as seen on the xz-plane. In (a), the contour of a generic original profile is highlighted (used is Figure 3a).

field, such as an electrical field. Using the proposed, generalized representation of the contact line, which is described next, the adhesion force was evaluated from simulated drops with the following geometries: (1) x-symmetric ellipsoid with semiaxes $a = 3, b = 1.3, c = 1$ rotated by 20° around the y-axis with respect to the canonical orientation; the ellipsoid was truncated by a horizontal plane (see Figure 4); (2) xy-symmetric ellipsoid with semiaxes $a = 4, b = 2, c = 2$; the ellipsoid was truncated in the lower part to reproduce contact angles higher than 90° and to emulate a drop on a hydrophobic surface (see Figure 5). Simulated experiments were performed for other geometries; however, since the general trend was similar, only results for the above two shapes have been reported here for brevity.

Once the synthetic drop geometry was defined, the image recording process was simulated. Just as a camera records a series of drop profile images by rotating around the drop in an actual experiment, profile images of the synthetic drop were created at different azimuthal angles. The construction of simulated profiles can be understood with the help of Figure 3a, in which the shape of the xy-symmetric synthetic drop, shown in Figure 5, was used.

At each line of sight for the camera, an original profile (thick line in Figure 3a) was identified. The recorded profile (outline of the shadowed area) was obtained as the projection of the original profile on the plane perpendicular to the line of sight for the camera. The simulation of the camera recording process was necessary to simulate perspective error, which has been described in the previous section.

The profile image series, whether obtained from actual or simulated experiments, were then used to infer a continuous representation of contact line and contact angle distribution. These representations were subsequently used to evaluate the drop adhesion force, as described in section 5.

5. IBAFA Methodology

The procedure for drop adhesion force evaluation can be divided into three steps: (1) the reconstruction of the contact line shape from the measured contact points, whose coordinates have been obtained from a series of profile images; (2) the extraction of the contact angles from the profile images and the determination of the contact angle distribution along the contact line; and (3) the calculation of the drop adhesion force, expressed by eq 6.

In the first step, the contact line shape reconstruction was tested both in actual experiments and in simulated experiments. In the experiments, profile images of a drop on a tilted surface were recorded by a camera and analyzed. The radii of the two contact points in each image were extracted (Figure 6). The x- and y-origins were set to the apex, since it is the only landmark that can be seen from every azimuthal viewing angle.

The procedure was also tested in simulated experiments, which offer the opportunity (1) to more precisely test the contact line reconstruction method on a variety of predefined drop shapes, without experimental limitations, and (2) to verify if the perspective error was corrected effectively; that is, if the corrected contact point coordinates, ($r_{\phi,C}$, ϕ_C), coincide with the original contact point coordinates (r_ϕ, ϕ).

The second step for IBAFA consists of the extraction of the contact angles from the profile images and the subsequent reconstruction of the contact angle distribution along the contact line. This procedure was tested in simulated experiments using synthetic drops. The advantage of testing the contact angle measurement procedure using synthetic drops is that the drop geometry is defined analytically and is therefore deterministically known. This is fundamental when it is necessary to evaluate the possible error sources. As an example, the issue of perspective error was carefully analyzed, since in refs 6 and 7 this issue was only partially explored. In the present study, measurement data can be directly compared to the analytical values and the adhesion force error can be exactly calculated, providing a quantitative estimation of perspective error influence on results.

The third step is the calculation of the drop adhesion force. Once the contact line and the contact angle distribution along the contact line are known, the drop adhesion force can be evaluated, according to eq 6. Generally, only the force in the x-direction (see Figure 1a) is of interest, since the net force on the y-direction, F_y, is null. However, since tests were performed on synthetic drops with at least one axis of symmetry, the integration of the forces was computed on one-half of the contact line. In this way, F_y will be nonzero and it can be used as additional information for the evaluation of the methodology. The evaluation of F_y may be of concern for generic nonsymmetric drops. Such drops can exist if the surface is irregular or if there is a surface energy gradient that is not aligned with the direction of the surface tilt. In this case, it can be valuable to calculate the F_y to verify if the assumed contact angle distribution correctly estimates a zero force in the y direction.

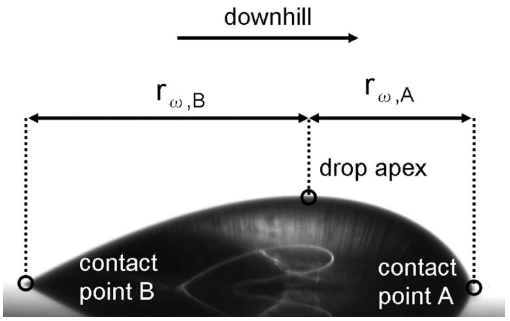

Figure 6. Example of profile image for a drop on a tilted surface. Note that the camera has been rotated in the same plane as the surface. Note that the camera is positioned with a tilt angle of approximately 1°−2° looking down onto the drop. This is to facilitate automatic identification of the contact point and the measurement of the contact angle from the profile images.

The forces F_x and F_y are defined as

$$\frac{F_{x,L/2}}{\gamma} = -\int_0^\pi \cos\theta(\phi)\cos\psi(\phi)\sqrt{r^2 + r'^2}\,\mathrm{d}\phi \qquad (7)$$

$$\frac{F_{y,L/2}}{\gamma} = -\int_0^\pi \cos\theta(\phi)\sin\psi(\phi)\sqrt{r^2 + r'^2}\,\mathrm{d}\phi \qquad (8)$$

where the adhesion forces were normalized with respect to γ in calculations and the subscript $L/2$ recalls that the integration is performed on half of the contact line (i.e., with the azimuthal angle, ϕ, ranging from 0 to π). The adhesion force value from eq 6, $F_{adhesion}$, is twice that of F_x. The numerical discretization of eqs 7 and 8 is described in section 5.3.

The adhesion force for synthetic drops on tilted surfaces was calculated using four different methodologies: (i) Assuming a circular contact line shape, $\theta = \theta_{max}$ on the leading half of the contact line and $\theta = \theta_{min}$ on the trailing half; this approach was proposed in ref 9 for bubbles; considering the F_x, this methodology is also equivalent to the model proposed in ref 3, where a drop contact line shape was represented by a leading and a trailing circular arc. (ii) Methodology from ref 5, assuming an elliptical contact line shape and a linear interpolation for the contact angle cosine distribution, $\cos\theta(\phi)$, given the maximum and minimum contact angle. (iii) Methodology from ref 6, assuming an elliptical contact line shape and a third order polynomial relation for the contact angle cosine distribution, $\cos\theta(\phi)$. (iv) IBAFA, which reconstructs the drop geometry from a series of profile images without any restrictive assumptions. Results were compared to the benchmark, which was the analytical force derived from the analytical expressions for contact line and contact angle from synthetic drops. Table 1 summarizes the characteristics of each of these methodologies.

This study should be seen as a comparison among different methodologies present in the literature and the introduction of a novel approach to evaluating the adhesion force. In this light, whether the Young−Laplace equation is satisfied is a moot point: this further justifies the choice of ellipsoids as numerical test cases.

5.1. Contact Line Shape Reconstruction. A top view of the contact line is not always available, as the contact line will be obstructed, wherever the contact angle exceeds 90°. Contact angles well beyond 90° are often encountered in studies of superhydrophobic surfaces.[21,22] In these situations, the contact line can

(21) Li, W.; Amirfazli, A. *J. Colloid Interface Sci.* **2005**, *292*, 195–201.
(22) Tavana, H.; Amirfazli, A.; Neumann, A. W. *Langmuir* **2006**, *22*, 5556–5559.

Table 1. Summary of the Characteristics of Different Adhesion Force Calculation Methodologies

methodology	contact line	contact angle distribution
(i) from ref 9	circular	leading half θ_{max} and trailing half θ_{min}
(ii) from ref 5	elliptical	$\cos\theta(\phi)$ linear function
(iii) from ref 6	elliptical	$\theta(\phi)$ third order polynomial
(iv) IBAFA	Fourier series	extracted from profile images

still be measured, by reconstructing it from a series of drop profile views, recorded by a camera revolving around the drop.

As was described previously, the contact points taken from profile views of the drop must be corrected for perspective error, but this correction requires a mathematical representation of the contact line shape. In ref 6, this correction was carried out while assuming that the contact line was an ellipse. In IBAFA, a more general representation of the contact line is proposed: a Fourier cosine series. This representation does not require any assumption on the contact line shape, in order to provide an analytical formulation. Thus, the contact line shape can be expressed as

$$r(\phi) = \sum_{j=0}^{n-1} a_j \cos(j\phi) \tag{9}$$

where n is the number of coefficients (a_j) used in the series. In using a cosine series, rather than a full Fourier series, the contact line is assumed to be symmetrical about the x-axis, which is often the case for drops placed on homogeneous surfaces and subjected to an external force in the x-direction. The assumption is made to save computational time, but including the sine terms is only a trivial matter.

It should be noted that the Fourier cosine series is a general representation that can be applied to any drop/bubble contact line shape, regardless of the liquid/gas/surface combination. In other words, there is no need to find and tune the most appropriate contact line shape for each specific case, as is done in the literature to date. No restricting or case specific assumption for the contact line shape is therefore required.

5.1.1. Fourier Cosine Series Algorithm. Given m points of the contact line and their original coordinates ($r_{\phi,i}$, ϕ_i) (see Figure 3), it is necessary to find n coefficients a_j, so that the cosine series best fits the data. Mathematically, since $m > n$, this is achieved by specifying an objective function, H, and optimizing it. The chosen objective function was the mean-square deviation between the contact point radius given by the cosine series $r(\phi_i)$ and the correct original contact point radius $r_{\phi,i}$:

$$H(a_j) = \sum_{i=1}^{m} \frac{\left(r(\phi_i) - r_{\phi,i}\right)^2}{m-1} = \sum_{i=1}^{m} \frac{\left(\sum_{j=0}^{n-1} a_j \cos(j\phi) - r_{\phi,i}\right)^2}{m-1} \tag{10}$$

The solution was performed in two ways: with a variable grid search method and by use of the built-in MatLab (The MathWorks, Inc.) function *fmincon*, which finds the constraint minimum of a function, H. Both methods have shown equivalent performance in terms of fitting the points and convergence characteristics.

To improve solution convergence, a convexity constraint was applied, meaning that the fitted contact line representation must be convex at all points. The convexity condition is not a restrictive assumption in practice, as it would not be possible to measure the contact angle or contact point position from a profile image of the drop if the contact line was concave at that point. This condition is mathematically expressed by the curvature $\kappa(\phi)$, which must be positive all along the contact line:

$$k(\phi) = \frac{r^2 + 2r'^2 - rr''}{\left(r^2 + r'^2\right)^{3/2}} > 0 \tag{11}$$

where

$$r' = r'(\phi) = \frac{dr}{d\phi} = \sum_{j=0}^{n-1} -a_j j \sin(j\phi) \tag{12}$$

$$r'' = r''(\phi) = \frac{d^2r}{d\phi^2} = \sum_{j=0}^{n-1} -a_j j^2 \cos(j\phi) \tag{13}$$

Several tests were performed both with ellipse and double-ellipse contact line shapes and different aspect ratios. The convexity constraint is particularly useful for highly elongated shapes (e.g., for an ellipse with semiaxes ratio $a/b > 2$), since areas of low curvature are present. If the constraint was not applied, the solution of the contact line reconstruction procedure could converge to incorrect shapes.

5.1.2. Correction of the Perspective Error. It has been previously discussed that the contact points, (r_ω, ω), recorded from the profile images, are merely a projection of the original contact points, (r_ϕ, ϕ), on the viewing plane (see Figure 3b); thus, the recorded points must be corrected for perspective error. Figure 7 shows how the contact line shape of an experimental drop (15 μL drop of bromonaphthalene on mill finished aluminum) will be represented, if not corrected for perspective error; the difference is substantial.

Since there are two unknowns ($r_{\phi,i}$, ϕ_i) for each ith recorded contact point, two equations must be defined. One is given by the simple trigonometric relationship (see Figure 3b)

$$r_\omega = r_\phi \cos(\phi - \omega) \tag{14}$$

whereas the second is derived by considering that r_ω should be perpendicular to the line of sight. By expressing the Cartesian derivative as a function of polar coordinates, this condition can be written as

$$-\frac{1}{\tan\omega} = \frac{r + r'\tan\phi}{-r\tan\phi + r'} \left(= \frac{dy}{dx}\right) \tag{15}$$

where r and r' are given by eqs 9 and 12.

Substituting eq 14 into eq 10, the functional H can be rewritten in terms of the recorded contact points, (r_ω,ω), as

$$H(a_j, \phi_i) = \sum_{i=1}^{m} \frac{\left(\sum_{j=0}^{n-1} a_j \cos(j\phi) - \frac{r_{\omega,i}}{\cos(\phi-\omega)}\right)^2}{m-1} \tag{16}$$

where it has been made explicit that H is a function of both a_j and ϕ_i for a given recorded contact point, (r_ω,ω). The problem is therefore to find the values of the cosine series coefficients, a_j, and the azimuthal angles, ϕ_i, which minimize the objective function, H, that is, eq 16. This minimization problem is further constrained

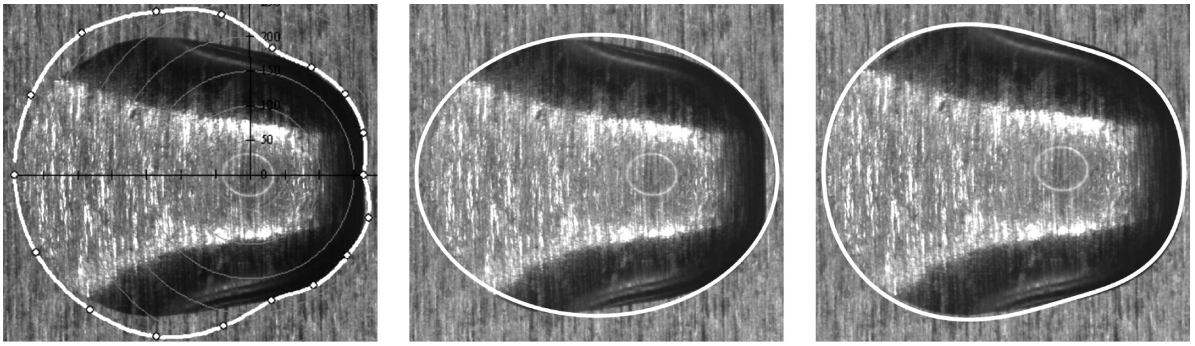

Figure 7. Reconstruction of the contact line shape shown in Figure 2b (15 μL drop of bromonaphthalene on mill finished aluminum) from a series of profile images. (a) Comparison between the original contact line shape and recorded contact line points. No correction is applied. Perspective error is not negligible. (b) Elliptical representation. (c) Fourier cosine series representation with five coefficients.

by eqs 11 and 15. Equation 15 was reformulated as follows for implementation:

$$\frac{\sum_{j=0}^{n-1} a_j \cos(j\phi) + \tan\phi \sum_{j=0}^{n-1} -a_j j \sin(j\phi)}{-\tan\phi \sum_{j=0}^{n-1} a_j \cos(j\phi) + \sum_{j=0}^{n-1} -a_j j \sin(j\phi)} + \frac{1}{\tan\omega} = 0 \quad (17)$$

5.2. Determination of the Contact Angle Distribution. The contact angle distribution along the contact line for a drop can be constructed from a series of profile images taken from various azimuthal positions. To extract contact angles from individual profile images, polynomial curves were fitted to the drop profile edge. The contact angles were then calculated from the slope of the fitted curves at the contact points. These contact angle measurements were assigned to the corresponding contact points ($r_{\phi,i}$, ϕ_i), which had been previously calculated during the perspective error correction procedure; the result is a discrete contact angle distribution. Particular attention was paid to perspective issues, both in the measurement of the contact angle and in the determination of the contact angle distribution along the contact line.

5.3. Numerical Discretization of Adhesion Force. The adhesion forces in the x- and y-direction, defined in eqs 7 and 8, were discretized for numerical computation as follows:

$$\frac{F_{x,L/2,\mathrm{num}}}{\gamma} = -\sum_{i=1}^{N_{\mathrm{int}}} \cos\theta_i \cos\psi_i \sqrt{r_i^2 + r_i'^2}\, \mathrm{d}\phi_i \quad (18)$$

$$\frac{F_{y,L/2,\mathrm{num}}}{\gamma} = -\sum_{i=1}^{N_{\mathrm{int}}} \cos\theta_i \sin\psi_i \sqrt{r_i^2 + r_i'^2}\, \mathrm{d}\phi_i \quad (19)$$

where the summation is done over the N_{int} integration points. Recall that the integration is only performed over half of the contact line, $L/2$. The integration was performed using two different integration step sizes: (1) a coarse integration, where the integration points coincide with the measured contact points, that is, $N_{\mathrm{int}} = n$, and (2) a fine integration, where the number of integration points is higher than that of the measured contact points, $N_{\mathrm{int}} > n$.

To perform the integration, one must provide the values of the normal to the contact line, ψ_i, the values of the contact angle, θ_i, the contact radius, r_i, and its derivative, r_i', associated with the ith integration point. For the coarse integration, the set of ψ_i, θ_i, r_i, and r_i' values is known, as the integration points coincide with the measured points and are provided by the profile image analysis. For the fine integration, a set of values needs to be interpolated between the measured points. As the contact line is known analytically, through the cosine series representation, the normal, ψ, the radius, r_i, and its derivative, r_i', can be defined in any point. The contact angle distribution along the contact line, $\theta(\phi)$, was found by a piecewise linear interpolation in the interval between the measured contact angles and evaluated at the integration points to give θ_i.

The results reported in this paper were obtained using 18 profiles and $N_{\mathrm{int}} = 181$, that is, fine integration method was used. These two values were chosen as a compromise between two competing requirements: using as little as possible profile images and obtaining an accurate value for the adhesion force. A more detailed discussion about the necessary number of profiles to reach the prescribed accuracy is reported in the Appendix.

After the image analysis process, the data extracted from the drop profile images are processed in a MatLab program to calculate the adhesion force. The structure of the code is simple and makes use of the built-in MatLab function, so that no particular numerical skills are required to implement the code. Also, the computational effort is not critical: on a typical PC, the data are processed in a few seconds to provide the value of the drop adhesion force.

6. Results and Discussions

6.1. Reconstruction of the Contact Line. In this section, the results for the reconstruction of the contact line are reported to demonstrate the application of the methodology. Results refer to both experiments and simulated experiments.

In Figure 7, the contact line of an experimental drop was reconstructed using either an ellipse (Figure 7b) or the cosine series with five coefficients (Figure 7c). The results show that the cosine series representation is capable of fitting the original contact line more accurately than the elliptical approximation, which is the most current method in the literature.

The methodology was also tested with simulated experiments on analytically known contact lines. As an example, the reconstruction of a double-ellipse contact line shape (as suggested in ref 6) is shown in Figure 8 (semiaxes: vertical $b = 2$, horizontal $a_{x<0} = 4$, $a_{x>0} = 1$). Results were obtained using 24 points, which represent the result of 12 profile images (each profile image

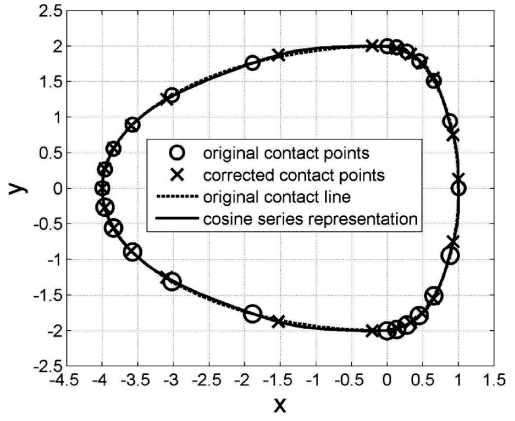

Figure 8. Reconstruction of a double-ellipse contact line (solid line), which coincides with the analytically defined double-ellipse contact line (dashed line) with semiaxes vertical $b = 2$, horizontal $a_{x<0} = 4$, $a_{x>0} = 1$. The symbols refer to original contact points (circle) used in simulated measurements and to contact points corrected for perspective error (crosses). The units are arbitrary.

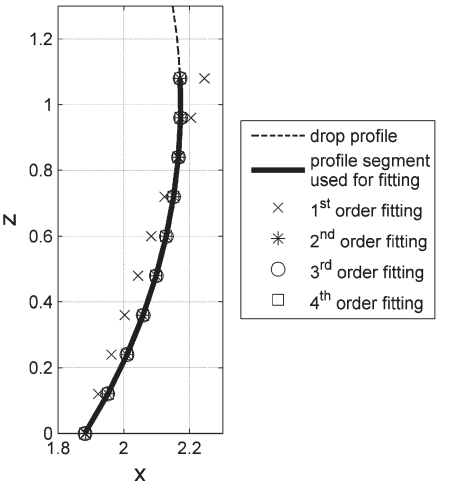

Figure 9. Profile of a drop with high contact angle, compared to different order polynomial fitted curves. Close up view near the contact point. The whole drop profile consisted of 50 points, of which 10 were used to fit the polynomials. The units are arbitrary. The directions x and z refer to coordinates as defined in Figure 1.

provides two contact point radii). From the recorded coordinates, both the overall shape of the contact line and the corrected position of the contact points ($r_{\phi,C}$, ϕ_C) were reconstructed. Figure 8 shows that the contact line, reconstructed using IBAFA, represents correctly the original points (analytically available), denoted by circles. However, Figure 8 shows that the reconstructed contact points (crosses), whose coordinates are ($r_{\phi,C}$, ϕ_C), do not all accurately coincide with the original contact points (circles), with coordinates (r_ϕ, ϕ). This is especially visible in those regions where the curvature is low. Note that this mismatch does not depend on the use of the cosine series representation. It is generally difficult to correct the perspective error on areas of low curvature independently from the chosen mathematical representation. Although corrected contact line points do not agree well with actual contact line points, Figure 8 clearly indicates that this issue does not significantly affect the representation of the contact line shape, since the corrected points all are in good agreement with the analytically constructed contact line. However, the determination of the contact angle distribution associated with these contact points would be misplaced, the possible consequences of which will be discussed in section 6.2.3.

6.2. Determination of the Contact Angle Distribution. In this section, the results obtained with IBAFA for determination of the contact angle distribution of synthetic drops, for both the *xy*-symmetric and *x*-symmetric cases, are presented. The contact angle distribution found using the present methodology is compared to that calculated analytically based on the predefined drop geometry.

6.2.1. xy-Symmetric Drop. Figure 9 shows a plot of a simulated drop profile near the contact line of the *xy*-symmetric synthetic drop from Figure 5. This segment of the profile was fitted with a polynomial, whose derivative at the contact point was then used to determine the contact angle. Each drop profile (dashed line in Figure 9) consisted of 50 points, of which 10 were used for fitting a polynomial (solid line).

The polynomial fit was assessed in terms of error in resultant contact angle measurements, with respect to the analytical solution. This assessment was carried out for first through fourth order polynomial fits, with the results shown in Figure 10a. Considering the maximum errors, whose values are reported in Table 2, and the necessity of keeping the order of the polynomial low, to avoid the possibility of fittings with spurious oscillations, a third order polynomial was deemed suitable, in accordance with ref 23.

6.2.2. x-Symmetric Drop. The results from the *x*-symmetric drop from Figure 4 were similar to those for the *xy*-symmetric drop. From the results depicted in Figure 10b, the contact angle is accurately evaluated using a polynomial fitting of at least the third order. The magnitude of error for different polynomial orders are similar to those obtained with the *xy*-symmetric shape (see Table 2).

An important result from these simulated experiments is that there is no imaging perspective issue related to the measurement of the contact angle from profile images/views. In other words, the value of the contact angle, that is extracted from a drop profile image, is not affected by perspective error and does not require any correction.

6.2.3. Contact Angle Distribution. Although there is no perspective issue in the measurement of the contact angle from profile views, as demonstrated by Figure 10, there may be an error in determining the local contact angle distribution along the contact line. This issue was alluded to in ref 7; that is, the correct measured value of the contact angle may be assigned to the wrong position on the contact line.

To understand the above issue, see Figure 8, which shows the reconstruction of a double-ellipse contact line. Although the overall contact line shape is well evaluated, in some areas there is a mismatch between the reconstructed contact points, whose coordinates are ($r_{\phi,C}$, ϕ_C), and the original contact points, whose coordinates are (r_ϕ, ϕ). This is observed particularly in the areas where the curvature is low. If in the low curvature area the contact angle gradient is low, the error from the contact point repositioning has a negligible influence. If the contact angle gradient is high, then the drop adhesion force can be evaluated with a higher error.

6.3. Force Calculation. Once the contact line shape and the contact angle distribution along the contact line are known, it is possible to calculate the force in the *x*- and *y*-directions, $F_{x,L/2}$ and $F_{y,L/2}$, respectively (see eqs 18 and 19).

(23) Bateni, A.; Susnar, S. S.; Amirfazli, A.; Neumann, A. W. *Colloids Surf., A* **2003**, *219*, 215–231.

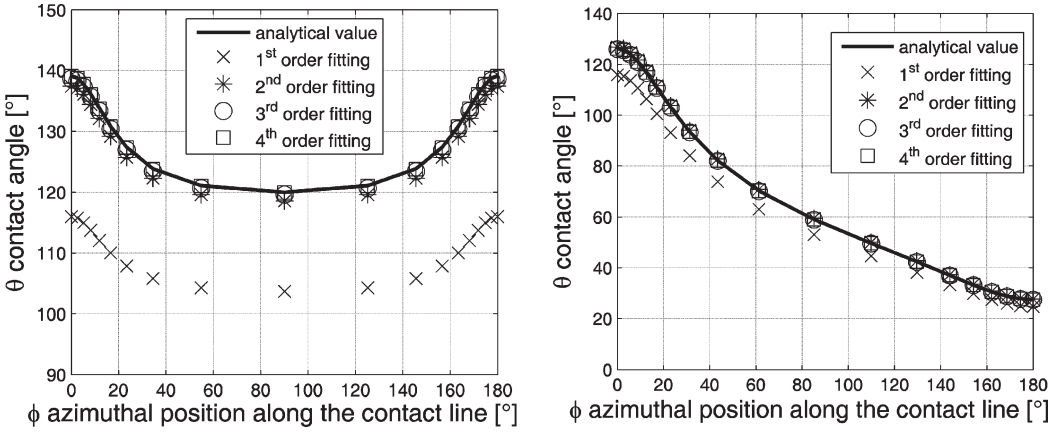

Figure 10. Determination of the contact angle distribution, using fitted polynomials of different orders, compared to the analytical solution, at different contact line azimuthal positions: (a) *xy*-symmetric drop (see Figure 5 for geometry details) and (b) *x*-symmetric drop (see Figure 4 for geometry details).

Table 2. Maximum Error for Determining the Contact Angle[a]

	error [%]			
drops	first order	second order	third order	fourth order
xy-symmetric	16.64	1.21	0.33	0.05
x-symmetric	14.22	0.52	0.16	0.03

[a] Polynomials of different order were used to approximate the drop profile. The analytical value of the contact angle, derived from the equation of the synthetic drop surface, was used as the benchmark.

Results were obtained with four different methodologies (see Table 1), for the *xy*-symmetric and for the *x*-symmetric synthetic drops. Methodologies (ii) and (iii) were computed using the analytical contact line, since this coincides with an ellipse. As the contact line is given, the errors due to an inappropriately modeled contact line and for perspective error were both zero. Thus, it was possible to independently estimate the error due to the simplifying assumptions for the contact angle distribution (e.g., cos $\theta(\phi)$ as linear or third order polynomial function).

6.3.1. xy-Symmetric Drop. The methodologies (i), (ii), and (iii) all assume that a single profile image can provide the maximum and minimum contact angles; that is, they can be found at the azimuthal angles $\phi = 0°$ and $\phi = 180°$, respectively. This is not the case for the *xy*-symmetric drop, where maximum and minimum contact angles are found at $\phi = 0°$ and $\phi = 90°$, respectively. Therefore, θ_{max} and θ_{min} must be extracted from two different images in practice. If a single image is used, it will appear that the contact angle is the same at $\phi = 0°$ and $\phi = 180°$ (see Figure 5) and it will be concluded that the contact angle is uniform along the contact line. However, a uniform distribution of the contact angle along the contact line does not represent the correct distribution.

For this reason, methodologies (i), (ii), and (iii) cannot be used to evaluate the adhesion force of a *xy*-symmetric drop. Only IBAFA was used for evaluating the forces on the *xy*-symmetric drop and compared to the analytical values.

For the *xy*-symmetric drop, $F_{x,L/2}$ was theoretically zero, as the drop is symmetric with respect to the *y*-axis: IBAFA evaluates it correctly, with negligible error (on the order of 10^{-4}). The results for $F_{y,L/2}$ show that IBAFA can evaluate the force with a small error (−0.30%) when compared to the analytical value.

6.3.2. x-Symmetric Drop. Considering the case of a drop subject to an external force, such as gravity, the *x*-symmetric drop case is more interesting than the previous one, as it is more representative of a distorted drop subjected to an external force.

Table 3. Adhesion Forces Obtained with the Methodologies Described in Table 1 for the *x*-Symmetric Synthetic Drop[a]

methodology	$F_{x,L/2}/\gamma$	e_x[%]	$F_{y,L/2}/\gamma$	e_y[%]
analytical	1.370		1.125	
methodology (i)	2.418	76.50	0.0468	−58.40
methodology (ii)	1.321	−3.56	0.598	−46.86
methodology (iii)	1.546	12.86	0.598	−46.86
IBAFA	1.369	−0.10	1.125	0.03

[a] The distribution of the normal $\psi(\phi)$ and of the contact angle $\theta(\phi)$ along the contact line is shown in Figure 11. Forces have been calculated on half of the contact line, $L/2$, and were normalized with respect to γ.

For a *x*-symmetric drop, both $F_{x,L/2}$ and $F_{y,L/2}$ are of interest, as they are both nonzero (over half of the contact line). Table 3 shows the results obtained with the four methodologies, and Figure 11 illustrates the distribution of $\psi(\phi)$ and $\theta(\phi)$. As for the *xy*-symmetric shape, IBAFA results are in very good agreement with the analytical ones, since the errors are lower than 0.1% for both force components. On the other hand, the methodology (i) evaluates the force inadequately, with an error of 76.5% for $F_{x,L/2}$. The other two methods, (ii) and (iii), provide results with low accuracy (see Table 3). The results in terms of $F_{y,L/2}$ are poorer, since the evaluated force is half the analytical value. It should be noted that methodologies (ii) and (iii) were taken from refs 5 and 6, for which $F_{y,L/2}$ may not have been relevant. In fact, they were more concerned with the evaluation of the force in the *x*-direction, that is, the direction of the gravity component along the surface. However, the error of the evaluated adhesion force is a direct consequence of an inaccurate description of the contact angle distribution along the contact line, regardless of *x*- or *y*-direction.

The reason for the low accuracy of methodology (iii) may be due to its range of applicability. In ref 6, where this methodology is taken from, it is shown that the third degree polynomial interpolation represents well the contact angle distribution along the contact line for a case with a small difference between the maximum and minimum contact angle ($\theta_{max} - \theta_{min} \approx 15°$). Also, it is reported that the maximum analyzed contact angle hysteresis, $\theta_A - \theta_R$, is 51°, but no value is reported for the maximum analyzed $\theta_{max} - \theta_{min}$. Thus, the methodology may not apply to this case, where $\theta_{max} - \theta_{min} \approx 100°$. On the contrary, IBAFA is shown to work for both small and large differences between θ_{min} and θ_{max}.

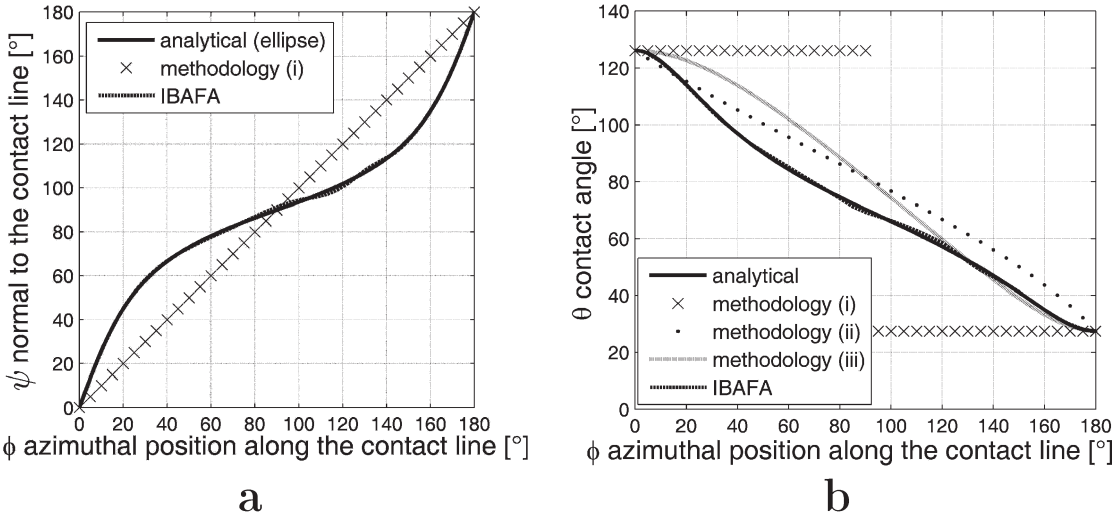

Figure 11. Distribution of geometrical properties along the contact line for the *x*-symmetric synthetic drop (see Figure 4): comparison between analytical values and results from different methodologies. (a) Normal to the contact line, $\psi(\phi)$ (note that for methodologies (ii) and (iii), the analytical expression was used). (b) Contact angle distribution along the contact line.

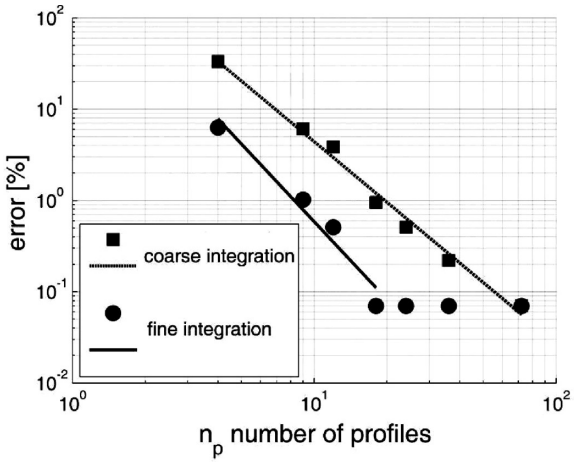

Figure 12. Error convergence for the drop adhesion force by increasing the numbers of profile images. Simulated experiments were performed on a synthetic drop. The adhesion force was calculated using IBAFA and then compared to the analytical values to evaluate the error. As an example, rotating the camera by 20° intervals over 180°, 9 profile images are obtained. The lines are to guide the eyes.

The errors obtained using methodologies (ii) and (iii) provide an estimation of the error, when the assumed contact angle distribution does not represent the actual contact angle distribution adequately. Note that in methodology (ii) the contact angle distribution is also arbitrarily selected, irrespective of the Young−Laplace equation. With regards to methodology (iii), the assumed contact angle distribution (third order polynomial) has been proposed to fit experimental data but does not necessarily satisfy the Young−Laplace equation, as well; it has been just a convenient model for a particular system. Thus, the assumed contact angle distribution may not apply to a generic drop. The effective error with experimental drops will strongly depend on the system studied; that is, for some liquid/surface combination, the methodologies may work well, and for some others they may not. Regarding the latter point, one needs to consider that methodologies (ii) and (iii) use an elliptical contact line and thus can describe the contact line of the proposed synthetic drop accurately, since this is also an ellipse. For a generic experimental drop, the contact line may significantly differ from an ellipse (see Figure 2), and the reported error may even increase further.

As a reference, the value of the fitting parameter k in eq 3 was derived for the *x*-symmetric drop. Using the analytical value of the force, the adjustable parameter k takes the value 1.18. As a reference length, an equivalent radius was used, that is, the radius of the circle with the same area as the contact surface.

The accuracy, by which the adhesion force is evaluated using IBAFA, allows its application to other problems. For example, determination of interfacial tension from tilt plate experiments. Consider a stationary drop on a tilted surface with a known mass. The gravity force is derived from the surface inclination and the mass. Since at the equilibrium condition the adhesion force is equal to the component of the gravity force along the surface, the liquid surface tension can be obtained using the inverse of procedure for IBAFA.

7. Conclusions

In this paper, a detailed description of a new methodology, IBAFA, for evaluating the adhesion force of a drop on a surface, subjected to an external force, is given. The methodology is based on the use of multiple profile images of a drop. The images are used to accurately reconstruct both the contact line shape and the contact angle distribution along the contact line. A general representation of the contact line shape is given by the use of the Fourier cosine series representation. Furthermore, the current formulation for the calculation of the adhesion force for drops with a noncircular contact line currently presented in literature is discussed and corrected.

The generality of the approach allows the methodology to be particularly suitable for the analysis of drops with highly "irregular" shapes, such as those encountered in industrial applications, where surfaces with anisotropic topography may be often involved.

The contact line shape reconstruction procedure was validated with both actual experiments and simulated experiments. The procedure for the calculation of the adhesion force was tested using simulated experiments with synthetic drops of known shapes.

One of the critical issues, connected to the use of multiple profile images, was perspective error. The Fourier series representation provides the required mathematical formulation for

correcting it. Perspective error plays instead no role in measurement of the contact angles from the profile images.

The results for the drop adhesion force demonstrated the capability of IBAFA to evaluate the adhesion force due to surface forces correctly, with a small error, generally in the order of 1%, when compared to the analytical results. This good agreement is a direct consequence of the capability of the new methodology to reconstruct the contact line shape and the contact angle distribution accurately and to correct the perspective error.

Different methodologies available in the literature[5,6,9] were also implemented, to provide the reader an estimation of the error, when simplifying assumptions, for example, circular and elliptical contact line, are invoked. The methodology from ref 9 provides results with a magnitude of the error in the order of 100%. The methodology from refs 5 and 6 leads to an error in the evaluation of the force up to 50%.

Acknowledgment. The authors acknowledge N. Glass for his technical support. The funding from the Natural Science and Engineering Research Council of Canada (NSERC), Discovery and DAS Programs, Canada Research Chair Program (A.A.), "I Plan de Iniciación a la I+D+I by Vicerrectorado de Investigación, Desarrollo e Innovación, UEx 2005" to "MEC-Plan Nacional I+D+I CICYT CTQ2006-01685/PP and JCyL VA116/A06" (F.J.C.), and Cariplo Foundation (A.A., C.A.) is acknowledged.

Minimum Number of Profiles. The methodology proposed in this paper, IBAFA, is based on the use of drop profile images. The images were used to reconstruct the contact line shape and the contact angle distribution accurately, so that an accurate evaluation of the drop adhesion force can be achieved.

For practical applications, such as industrial ones, it is needed to determine how many profiles are needed to obtain a evaluation of the adhesion force within a prescribed accuracy. A compromise should be found between two competing requirements: the accuracy of the evaluation and the number of images that can be recorded and analyzed to obtain the information on the contact line and the contact angle distribution.

The error from using the proposed methodology in evaluating the adhesion force of the drop, compared to the analytically derived value, was calculated for different drop shapes, using a variable number of profile images. The adhesion force was computed according to eqs 18 and 19. The calculation was performed using two different integration step sizes, labeled as coarse and fine integration. For the coarse integration, the number of integration points N_{int} was equal to the number of profiles n. For the fine integration, the number of integration points was set equal to 181.

Figure 12 illustrates the percentage error in the evaluation of the adhesion force by using a variable number of profiles. Results refer to the x-symmetric drop (see Figure 4). As a general trend, an increase in the number of profiles reduces the error, which logarithmically decreases both for the coarse and for the fine integration. Furthermore, the fine integration provides better results compared to the coarse integration, using the same number of profiles. As an example, by recording 10 images, the error would be approximately 1% for the fine integration and 6% for the coarse integration. Finally, Figure 12 shows that it is unnecessary to record more than 18 profile images of the drop if the fine integration is used, as the error would no longer decrease for increasing number of recorded images. When 18 profiles are used, the error reaches a minimum value. This minimum is due to the accuracy in measuring the contact angle from the profile image. As reported in Table 2, the maximum error in measuring the contact line is 0.3% for a third order polynomial. Due to this limitation in the measurement process, even if the number of profile is increased to over 18, the error cannot be further reduced. For the coarse integration, the minimum error (0.07%) is reached with 70 profiles.

It can be concluded that the fine integration offers much more accurate evaluations than the coarse integration, with little extra computational effort. Furthermore, from this test and several others, which were not reported here, it was observed that approximately 9 profile images (i.e., one image every 20°) can be a good compromise between the necessity of accurate force evaluation ($e \approx 1\%$) and the use of a limited number of profiles. A smaller number of profiles could be used, if a lower accuracy was acceptable.